

Article

Easy Ligand Activation in the Coordination Sphere of Ru inside the $[PW_{11}O_{39}]^{7-}$ Backbone

Anna A. Mukhacheva ¹, Artem L. Gushchin ¹, Vadim V. Yanshole ^{2,3}, Pavel A. Abramov ^{1,4} and Maksim N. Sokolov ^{1,*}

¹ Nikolaev Institute of Inorganic Chemistry, Siberian Branch of Russian Academy of Sciences, 3 Akad. Lavrentiev Ave., 630090 Novosibirsk, Russia; anna-mukhacheva@mail.ru (A.A.M.); gushchin_al@yahoo.com (A.L.G.); abramov@niic.nsc.ru (P.A.A.)

² International Tomography Center SB RAS, Institutskaya str. 3a, 630090 Novosibirsk, Russia; vadim.yanshole@tomo.nsc.ru

³ Novosibirsk State University, Pirogova str. 2, 630090 Novosibirsk, Russia

⁴ South Ural State University, Prospekt Lenina 76, 454080 Chelyabinsk, Russia

* Correspondence: caesar@niic.nsc.ru

Academic Editor: Andrey I. Poddel'sky

Received: 30 March 2020; Accepted: 14 April 2020; Published: 17 April 2020

Abstract: Irradiation of the Keggin-type $[PW_{11}O_{39}\{Ru(NO)\}]^{4-}$ (**Ru-NO**) polyoxometalate in CH_3CN results in rapid NO ligand elimination with the formation of $[PW_{11}O_{39}\{Ru^{III}(CH_3CN)\}]^{4-}$ (**Ru-CH₃CN**). This complex offers an easy entry into the Ru-based chemistry of the $\{PW_{11}Ru\}$ complex. Attempts to substitute N_3^- for CH_3CN in the presence of an NaN_3 excess lead a variety of products: (i) $[PW_{11}O_{39}\{Ru^{III}(N_3)\}]^{4-}$ (**Ru-N₃**); (ii) $[PW_{11}O_{39}\{Ru^{III}(N_4HC-CH_3)\}]^{4-}$ (**Ru-Tz**) as a click-reaction product; and (iii) $[PW_{11}O_{39}\{Ru^{II}(N_2)\}]^{5-}$ (**Ru-N₂**). UV-VIS, CV, and HR-ESI-MS techniques were used for the reaction monitoring and characterization of the products.

Keywords: ruthenium; polyoxometalate; azide; CV; HR-ESI-MS

1. Introduction

Chemistry of noble-metal-substituted polyoxometalates, apart from general chemical interest of bringing noble metal centers in coordination to what can be regarded as noninnocent multidentate oxygen-donor ligand, is important for the search of new pathways of coordinated molecules activation and design of new catalysts, including photo- and electrocatalysts.

Of the polyoxometalates (POMs) incorporating noble metals, the most studied are Ru-substituted Keggin-type heteropolytungstates, where a $\{W=O\}^{4+}$ moiety in the plenary Keggin archetype, $[XW_{12}O_{40}]^{n-}$ ($X = P$ ($n = 3$), Si and Ge ($n = 4$)), is substituted by a $\{RuL\}$ group. L can be neutral or charged, such as O^{2-} or N^{3-} , and Ru in POMs is known to exist in at least five oxidation states, ranging from Ru(II) to Ru(VI). Incorporation of Ru confers unique redox and catalytic properties on the resulting POMs [1,2]. Catalytic activities of $[PW_{11}O_{39}Ru^{III}(H_2O)]^{4-}$, $[PW_{11}O_{39}Ru^{II}(DMSO)]^{5-}$ (DMSO: dimethyl sulfoxide), $[SiW_{11}O_{39}Ru^{III}(H_2O)]^{5-}$, $[SiW_{11}O_{39}Ru^{III}(DMSO)]^{5-}$, and $[GeW_{11}O_{39}Ru^{III}(H_2O)]^{5-}$ in oxidation of olefins [3–5], water [6–8], DMSO [9,10], and alcohols [11,12]; reduction of DMSO [10] and carbon dioxide [13]; and oxidative C–C bond formation [14] have been reported. The H_2O ligand attached to Ru is exchangeable with other organic and inorganic donor molecules to form **Ru-pyridine** [10,15,16], **Ru-pyrazine** [12], **Ru-DMSO** [10,17,18], **Ru-NO** [19–21], **Ru-Cl** [22], **Ru-CO** [23–25], **Ru-olefin** [10], and **Ru-O-Ru** derivatives [26,27].

In 2013 we reported incorporation of a $\{Ru(NO)\}^{3+}$ group into a Keggin type POM, $[PW_{11}O_{39}]^{7-}$, and versatile reactivity of the coordinate NO ligand [20,21]. Easily available $[Ru(NO)Cl_5]^{2-}$ offers serious advantages as Ru source for preparation of Ru-substituted Keggin-type heteropolytungstates

due to the redox stability of the $\{\text{Ru}(\text{NO})\}^{3+}$ unit, hydrolytic inertness, and consequent lack of uncontrollable hydrolytic oligomerization, though the inertness of coordinated Cl ligands in this low-spin d^6 -Ru(II) complex requires drastic reaction conditions. The coordinated NO can be destroyed or eliminated, leaving a vacant coordination site, which can open a way for activation of different substrates in catalytical applications [28–30]. Recently, we reported the reactions of $[\text{Ru}(\text{NO})\text{Cl}_5]^{2-}$ with pseudotrivalent B- α - $[\text{XW}_9\text{O}_{33}]^{9-}$ ($X = \text{As}^{\text{III}}, \text{Sb}^{\text{III}}$) at 160 °C resulting in rearrangement of the polyoxometalate backbones into $\{\text{XM}_{18}\}$ structures [31]. In the case of $[\alpha\text{-B-AsW}_9\text{O}_{33}]^{9-}$, oxidation of As(III) to As(V) took place, accompanied by rearrangement into Dawson type $[\text{As}_2\text{W}_{17}\{\text{Ru}(\text{NO})\}\text{O}_{61}]^{7-}$. In the case of $[\alpha\text{-B-SbW}_9\text{O}_{33}]^{9-}$, the product $[\text{SbW}_{17}\{\text{Ru}(\text{NO})\}\text{O}_{59}]^{10-}$ was isolated as $(\text{DMAH})_{10}[\text{SbW}_{17}\{\text{Ru}(\text{NO})\}\text{O}_{59}] \cdot 11\text{H}_2\text{O}$.

Another aspect highlighted here is reactions of coordinated ligands [32] or ligand activation in the coordination sphere of noble metals. Numerous research papers have been published in this field. Specifically we would like to highlight the reactivity of coordinated nitriles in the Pt coordination sphere [33–37] or reactivity of triosmium clusters toward a wide range of substrates [38–41]. UV-irradiation (or photolysis) is a well-known technique for a lot of chemical processes, including (i) ligand exchange reactions (e.g., low-valence iron, osmium clusters) [42,43], (ii) ligand transformation [44–46], and (iii) CO_2 capture [47].

Here, we report an easy way to remove the NO ligand from $[\text{PW}_{11}\text{O}_{39}\{\text{Ru}(\text{NO})\}]^{4-}$, quantitative generation of $[\text{PW}_{11}\text{O}_{39}\{\text{Ru}^{\text{III}}(\text{CH}_3\text{CN})\}]^{4-}$, and its reactions with N_3^- which follow three different pathways.

2. Results

Coordinated NO (formally, NO^+) ligand in the $\{\text{Ru}(\text{NO})\}^{3+}$ complexes typically can play three roles: (i) stabilizing low-spin d^6 -Ru(II) and imparting stability and inertness on the coordination sphere; (ii) acting as spectator ligand, capable of taking up or releasing extra electron density on Ru due to π -backbonding; (iii) easy transformations or elimination (releasing a coordination site) upon irradiation or in the presence of reducing agents or nucleophiles. In this work we used mercury lamp irradiation to eliminate NO ligand from $[\text{PW}_{11}\text{O}_{39}\{\text{Ru}(\text{NO})\}]^{4-}$ (**Ru-NO**) (Figures S1–S3, Table S1) in CH_3CN solution producing corresponding $[\text{PW}_{11}\text{O}_{39}\{\text{Ru}^{\text{III}}(\text{CH}_3\text{CN})\}]^{4-}$ anion. The reaction can be viewed as dissociation of neutral NO molecule with the formation of coordinatively unsaturated species $[\text{PW}_{11}\text{O}_{39}\{\text{Ru}^{\text{III}}\}]^{4-}$, followed by rapid solvation with CH_3CN , quantitatively yielding $[\text{PW}_{11}\text{O}_{39}\{\text{Ru}^{\text{III}}(\text{CH}_3\text{CN})\}]^{4-}$ (**Ru-CH₃CN**). This process was followed by IR, UV-VIS, and CV techniques.

After 90 min irradiation of a solution of **Ru-NO** in CH_3CN , the UV-VIS spectrum changed (Figure 1) by disappearance of the band at 412 nm ($\epsilon = 1059 \text{ M}^{-1}\text{cm}^{-1}$), and appearance of two new bands at 356 nm ($\epsilon = 2843 \text{ M}^{-1}\text{cm}^{-1}$) and 410 nm ($\epsilon = 1720 \text{ M}^{-1}\text{cm}^{-1}$). Cyclic voltammetry (CV) can be used for the monitoring of the substitution of CH_3CN for NO by following the change in the corresponding redox processes. The CV plot of **Ru-CH₃CN** in acetonitrile is shown in Figure 2. Three redox processes at $E_{1/2} = 0.92, -0.33$ and -1.64 V (vs. Ag/AgCl) were detected. The difference between the anodic and cathodic peak potentials (ΔE) does not exceed 80 mV, and the ratio between the anodic and cathodic peak currents (I_a/I_c) is close to 1 for each of these processes. All this indicates the reversibility of the processes. The oxidation process at 0.92 V corresponds to Ru(II)/Ru(III) couple. It was previously found that a similar **Ru-NO** complex reversibly oxidizes at 1.29 V (vs. Ag/AgCl) [20]. Two redox processes at -0.33 and -1.64 V should correspond to the reduction of W(VI) in the $\{\text{PW}_{11}\}$ framework, as is well documented.

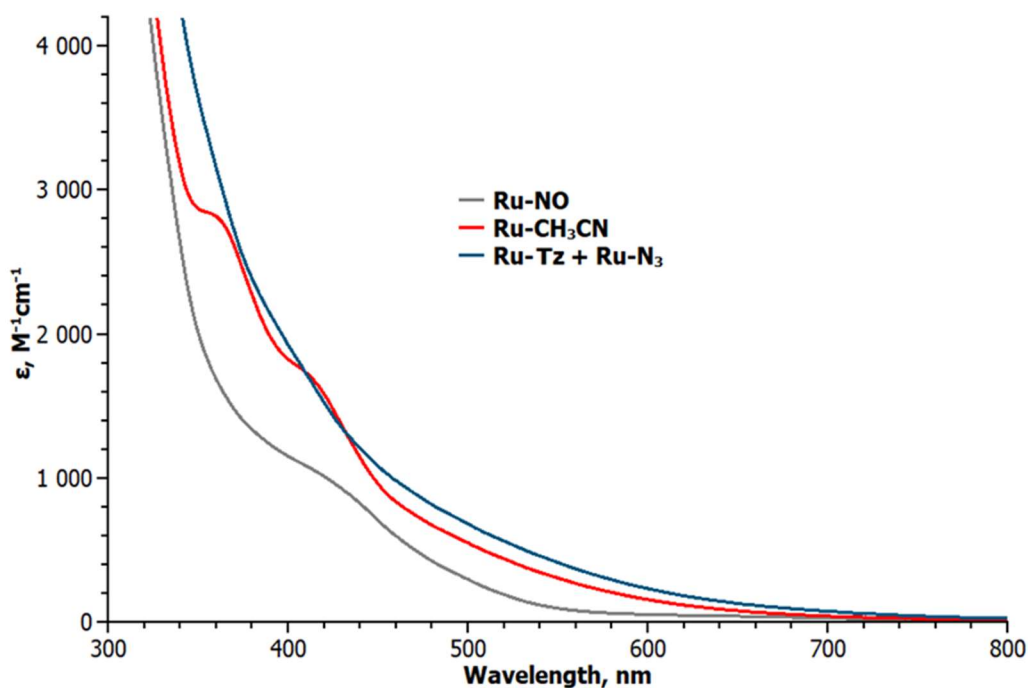


Figure 1. UV-VIS spectra for POM-Ru derivatives.

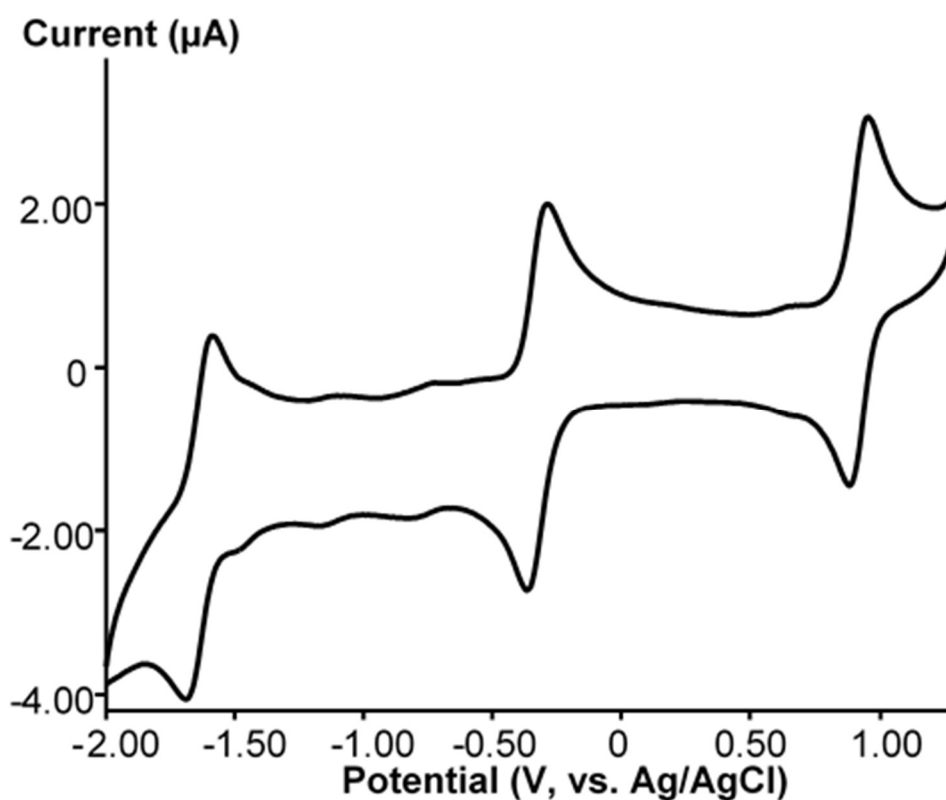


Figure 2. CV of Ru-CH₃CN in CH₃CN at scan rate of 100 mV/s.

The Ru-CH₃CN complex can be isolated as TBA-salt by diethyl ether diffusion for crystalline sample or bulk ether precipitation of the crude product. IR-spectroscopy confirms absence of NO ligand by disappearance of the tell-tale NO band at 1846 cm⁻¹ (Figures S7 and S8).

Ru-CH₃CN was prepared to study reactivity at the Ru site in various reactions. We tried to exchange the coordinated acetonitrile molecule with azide ligand in order to make the [PW₁₁O₃₉Ru^{III}(N₃)]⁵⁻ (**Ru-N₃**) complex and to study the reactions of the coordinated azide ligand. The reaction was monitored by CV. Heating of **Ru-CH₃CN** with a large excess of NaN₃ results in the changing of the UV-VIS spectrum (Figure 1). The spectrum differs from that of **Ru-CH₃CN** or **Ru-NO** and looks essentially featureless. The implicit absorption bands could be identified by calculating wavelength derivatives [48]. Two bands at 366 nm ($\epsilon = 2888 \text{ M}^{-1}\text{cm}^{-1}$) and 415 nm ($\epsilon = 1633 \text{ M}^{-1}\text{cm}^{-1}$) were detected (Figure S9). Substitution of acetonitrile leads to a noticeable cathodic shift in the Ru(II)/Ru(III) potential from 0.92 V (red line in Figure 3) to 0.57 V (black line in Figure 3). Additionally two small irreversible shoulders were detected. However, within the concentrations of NaN₃ employed in this work, we were unable to achieve complete substitution of CH₃CN by azide by working in CH₃CN. However, with large excess in NaN₃, the cyclic voltammogram plot shows the presence of three reversible Ru(II)/Ru(III) waves in the positive region (Figure 4). The first one corresponds to the formation of the azide complex, and the second one corresponds to the unreacted acetonitrile complex.

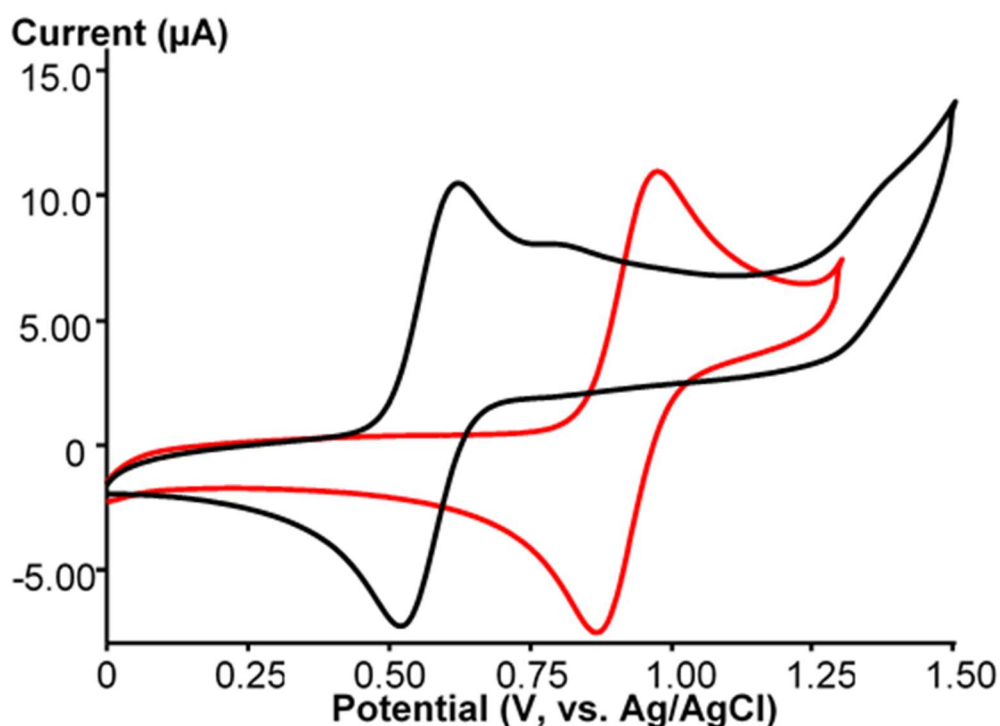


Figure 3. CVs of **Ru-N₃/Ru-Hc** (black line) and **Ru-CH₃CN** (red line) in CH₃CN in the range from 0 to 1.50 V at potential scan rate of 100 mV/s.

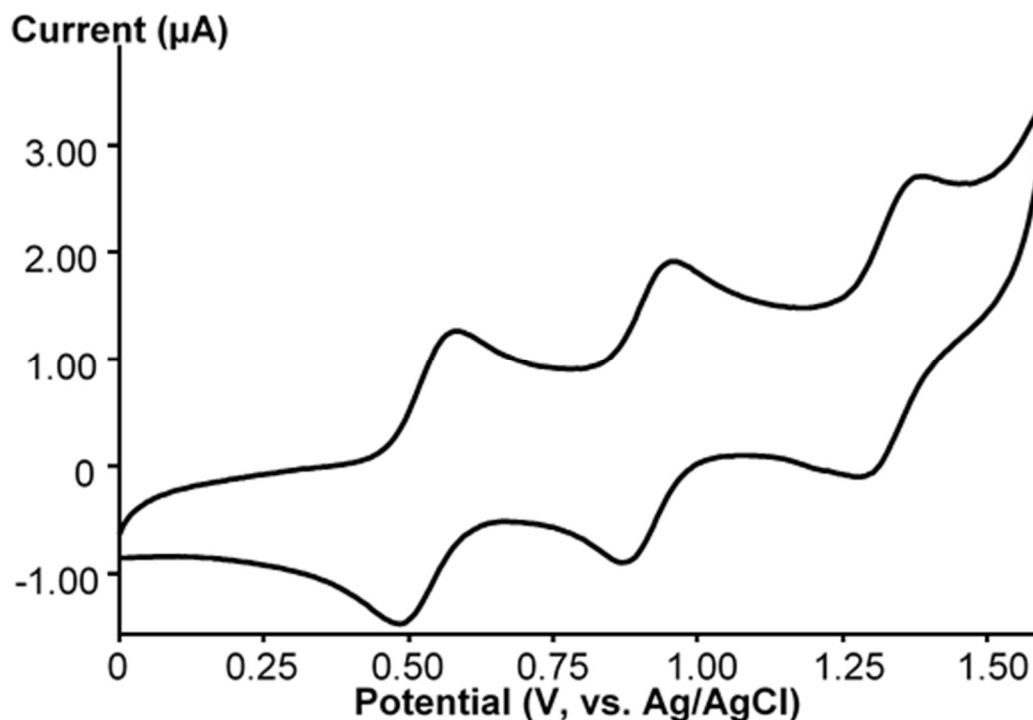


Figure 4. CV of the reaction mixture in CH_3CN in the range from 0 to 1.60 V at potential scan rate of 100 mV/s.

The composition of the complex was confirmed with elemental analysis and HR-ESI-MS (Figures 5, S4–S6, Table S2). We also used HR-ESI-MS techniques to study these reactions. The products were isolated by diethyl ether precipitation as mixtures of TBA salts and redissolved in CH_3CN for the measurements. The spectra (Figures 5, S10–S15, Table S3) indicate the presence of both **Ru-N₃** and **Ru-CH₃CN** complexes. Moreover, there are other species, such as $\{2\text{H}^+ + \text{Ru-N}_3 + \text{CH}_3\text{CN}\}^{3-}$ (m/z 954.451), $\{\text{Na}^+ + \text{H}^+ + \text{Ru-N}_3 + \text{CH}_3\text{CN}\}^{3-}$ (m/z 961.779), or $\{2\text{Bu}_4\text{N}^+ + \text{Ru-N}_3 + \text{CH}_3\text{CN}\}^{3-}$ (m/z 1115.424) (Table S3). Since an acetonitrile molecule is routinely required for matching calculated and experimental m/z values, this can be attributed to the formation of **N₄HC-CH₃** (**Tz**) tetrazole or tetrazolate (**Tz⁻**) in the coordination sphere of ruthenium as a click reaction result ([2 + 3] dipolar addition of azide to the nitrile bond). We have to conclude that the formation of **Ru-N₃** and $[\text{PW}_{11}\text{O}_{39}\{\text{Ru}^{\text{III}}(\text{N}_4\text{HC-CH}_3)\}]^{4-}$ (**Ru-Tz**) anion occurred during the reaction.

When the reaction is carried out in a weakly coordinating CH_3NO_2 , the HR-ESI-MS data (Figures 5, S16–S21, Table S4) reflect different pathways of ligand transformation. There are two products, with one of them being the above-mentioned **Ru-Tz** complex. This $[\text{PW}_{11}\text{O}_{39}\{\text{Ru}^{\text{III}}(\text{N}_4\text{HC-CH}_3)\}]^{4-}$ (**Ru-Tz**) was detected in the composite peaks $\{2\text{Bu}_4\text{N}^+ + \text{Ru-Tz}\}^{2-}$ (m/z 1673.633) and $\{2\text{Bu}_4\text{N}^+ + \text{Ru-Tz} + \text{H}_2\text{O}\}^{2-}$ (m/z 1682.642).

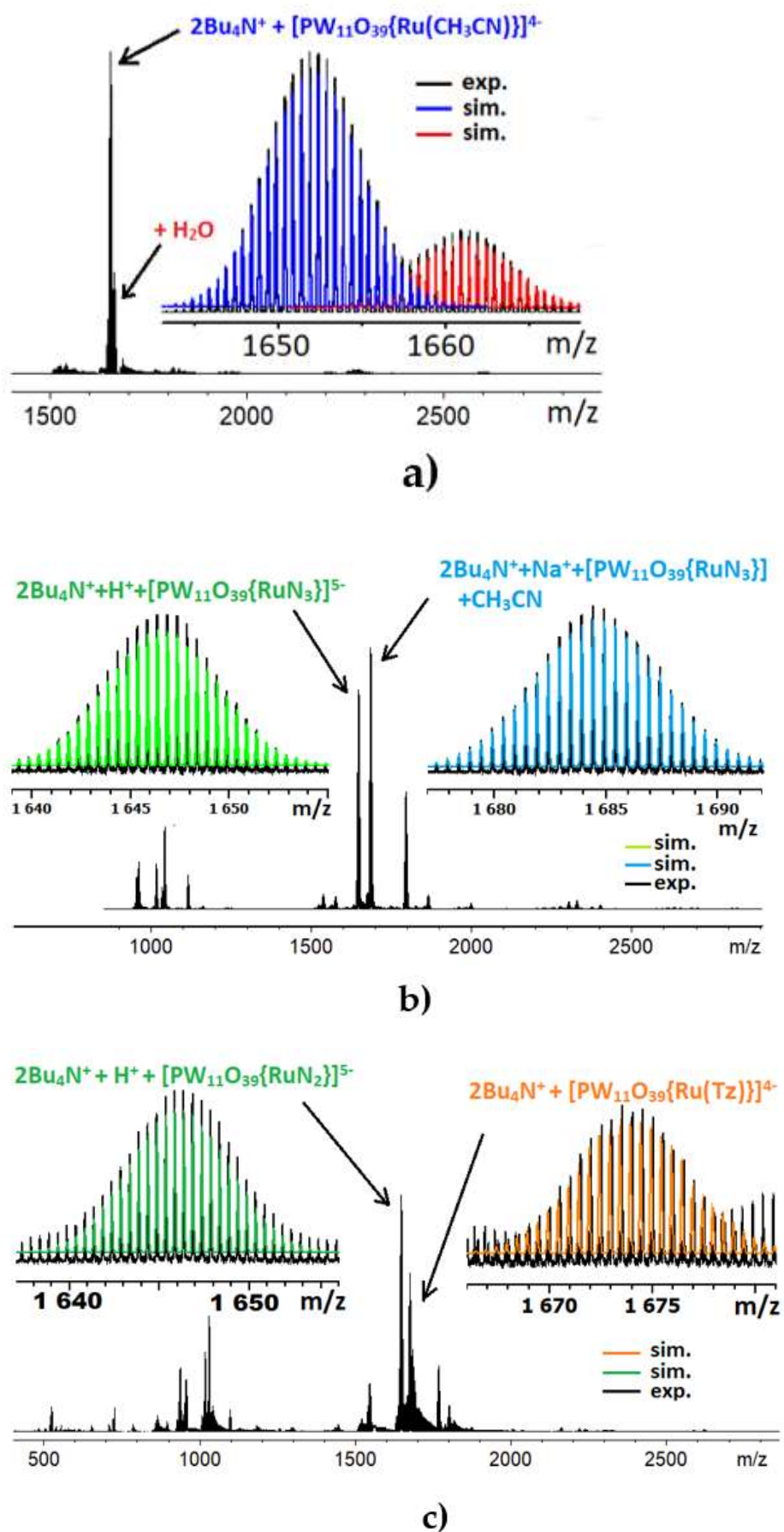


Figure 5. HR-ESI-MS spectra of Ru-CH₃CN (a), Ru-N₃ (b), Ru-N₂ and Ru-Tz (c).

We can conclude that activation of azide ligand in the coordination sphere of Ru leads to a fast reaction with CH_3CN into the tetrazole molecule. We proposed the following mechanism of this reaction (Figure 6).

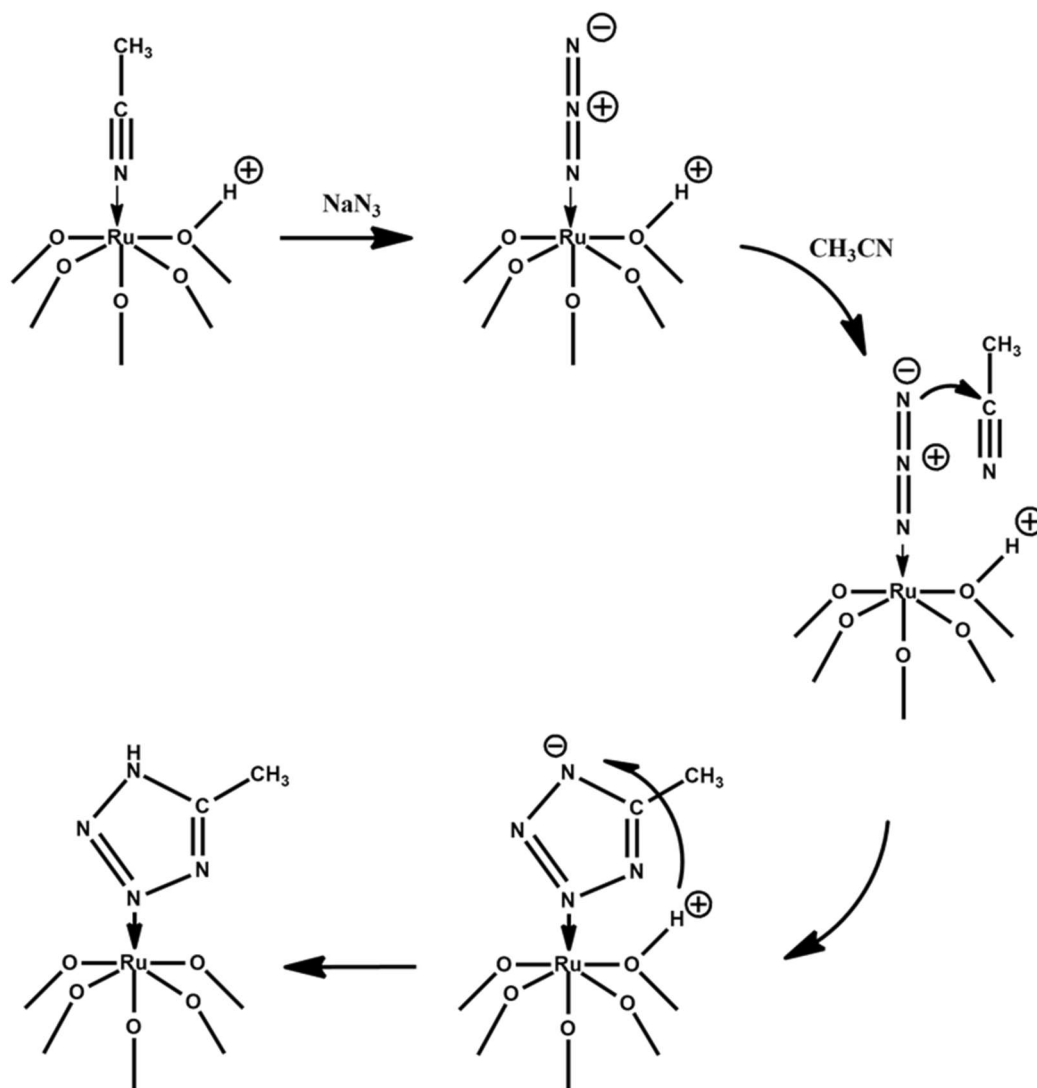
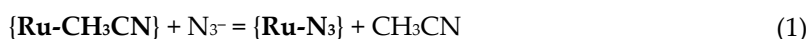


Figure 6. The proposed mechanism of N_3^- and CH_3CN coupling in the coordination sphere of Ru.

In the CH_3CN solution, and in the presence of excess azide, there are competing reactions leading to $\text{Ru}-\text{N}_3$ and $\text{Ru}-\text{CH}_3\text{CN}$ complexes. These are not possible in CH_3NO_2 when stoichiometric amounts of azide are employed.

The azide–alkyne Huisgen cycloaddition is a 1,3-dipolar cycloaddition between an azide and a terminal or internal alkyne to give a 1,2,3-triazole [49]. Typically, such reactions can be catalyzed by Cu(I) [50], Ru [51,52], and Ag(I) [53,54]. The Ru-based catalysts are typically low-valent organometallic complexes like $[\text{Cp}^*\text{RuCl}(\text{PPh}_3)_2]$, $[\text{Cp}^*\text{RuCl}(\text{COD})]$, and $[\text{Cp}^*\text{RuCl}(\text{NBD})]$ [52]. The ruthenium-catalyzed azide–alkyne cycloaddition proceeds by an oxidative coupling of the azide and alkyne to give a six-membered ruthenacycle intermediate, in which the first new carbon–nitrogen bond is formed between the more electronegative carbon of the alkyne and the terminal, electrophilic nitrogen of the azide. In our case POM plays the role of a bulky ligand with “hard” oxo-environment, and ruthenium has 3+ oxidation state. This nonfavorable arrangement can induce partial leaving of a noble metal atom from the POM lacuna to achieve the suitable geometry for oxidative addition. The above-mentioned mechanism does not include changing of the Ru coordination environment and can be more favorable.

Moreover, analysis of the HR-ESI-MS data reveals another product in the reaction mixture in CH_3NO_2 . The m/z calculations suggest coordination of the $\{\text{PW}_{11}\text{O}_{39}\text{Ru}\}$ moiety with a ligand of molecular weight between 28 and 30, which can be addressed to CO, NO, or N_2 . However, CH_3NO_2 cannot be a source of NO or CO under reaction conditions and most likely is not involved in the reaction. We are to assume, therefore, that this ligand comes from azide, and can be nothing except N_2 , attached to Ru^{II} (Figure 5). To confirm this, we studied the bulk solid mixture with Raman spectroscopy and found a band at 2135 cm^{-1} (Figure S22). Stable Ru^{II} complexes with coordinated N_2 molecule have been reported since the 1960s, including the first examples of dinitrogen complexes, isolated as $[\text{Ru}(\text{NH}_3)_5\text{N}_2]\text{X}_2$ ($\text{X} = \text{Br}^-, \text{I}^-, \text{BF}_4^-, \text{PF}_6^-$) [55]. According to the Raman data, the N_2 stretches can lie between 2103 cm^{-1} (for *trans*- $[\text{RuN}_3(\text{N}_2)(\text{en})_2]\text{PF}_6$ [56]) and 2140 cm^{-1} (for $[\text{Ru}_2\text{H}_6\text{N}_2(\text{PPh}_3)_4]$ [57]). Therefore, based on the HR-ESI-MS and Raman data, we can suggest formation of $[\text{PW}_{11}\text{O}_{39}\{\text{Ru}^{\text{II}}(\text{N}_2)\}]^{5-}$ complex following N_3^- activation upon coordination to the $\{\text{PW}_{11}\text{O}_{39}\text{Ru}\}$. The formation of the $[\text{PW}_{11}\text{O}_{39}\{\text{Ru}^{\text{II}}(\text{N}_2)\}]^{5-}$ can be rationalized by the following simplified scheme:



After detection of $\text{Ru}-\text{N}_2$ complex in the mixture of products isolated after the reaction in CH_3NO_2 , we checked a mixture isolated from acetonitrile and found peaks from the same complex with nitrogen. This means that heating of $\text{Ru}-\text{CH}_3\text{CN}$ with azide induces two parallel reactions of activated azide, resulting in tetrazole formation or nitrogen stabilization. The $[\text{PW}_{11}\text{O}_{39}\text{Ru}^{\text{III}}(\text{N}_3)]^{5-}$ complex must be considered as a highly reactive intermediate.

3. Materials and Methods

$\text{K}_2[\text{RuNOCl}_5]$ was prepared according to the literature [58]. IR spectra were recorded on a FT-801 FT-IR spectrometer (Simex, Russia). Elemental analysis was carried out on a Eurovector EA 3000 CHN analyzer. The TGA measurements were performed on a NETZSCH TG 209 F3 thermobalance in aluminum crucibles while heating the samples from 30 to $300\text{ }^\circ\text{C}$ at a step of $10\text{ }^\circ\text{C}$. A 1.5 kW full-spectrum Hg lamp (GO Pnik, Iskitim, Russia) was used for the bulk solution photolysis.

The cyclic voltammograms (CV) were recorded with a 797 VA Computrace system (Metrohm, Zurich, Switzerland). All measurements were performed with a conventional three-electrode configuration consisting of glassy carbon working and platinum auxiliary electrodes and an Ag/AgCl/KCl reference electrode. The solvent used in all experiments was CH_3CN , which was deoxygenated before use. Tetra-*n*-butylammonium hexafluorophosphate (0.1 M solution) was used as a supporting electrolyte. The concentration of the complexes was approximately 10^{-3} M . The potential scan rate was 100 mV/s . The half-wave potential ($E_{1/2}$) values were determined as $(E_a + E_c)/2$, where E_a and E_c refer to anodic and cathodic peak potentials, respectively. Ferrocene was used as an internal standard, and the Fc/Fc^+ potential was 0.43 V .

The high-resolution electrospray ionization mass spectrometric (HR-ESI-MS) measurements were performed at the Center of Collective Use "Mass Spectrometric Investigations" SB RAS (Novosibirsk, Russia). Spectra were obtained with a direct injection of liquid samples on an ESI quadrupole time-of-flight (ESI-q-TOF) high-resolution mass spectrometer Maxis 4G (Bruker Daltonics, Bremen, Germany). The spectra were recorded in the $300\text{--}3000\text{ }m/z$ range in negative mode.

Raman spectra were recorded on a LabRAM Horiba spectrometer (Horiba, Kyoto, Japan). An ion He-Ne laser (Simex, Moscow, Russia) with a wavelength of exciting light of 633 nm was used. The spectra were obtained in the backscattering geometry using a Raman microscope.

Synthesis of $(\text{Bu}_4\text{N})_4[\text{PW}_{11}\text{O}_{39}\{\text{Ru}(\text{NO})\}]$ ($\text{Ru}-\text{NO}$): 1 g (0.31 mmol) $\text{K}_7[\text{PW}_{11}\text{O}_{39}]\cdot 14\text{H}_2\text{O}$ was dissolved in 15 mL H_2O . Then, the solution of 0.132 g (0.31 mmol) $\text{K}_2[\text{RuNOCl}_5]$ in 1 mL H_2O was added. The resulting mixture was transferred into a Teflon-lined Parr autoclave and kept at $150\text{ }^\circ\text{C}$ for 18 h. After cooling to the room temperature, TBABr was added (1 g, 0.95 mmol). The precipitation was filtered

on a glass filter and rinsed with 200 mL of a distilled water. Yield: 1.070 g (95%). ^{31}P NMR ($\text{CH}_3\text{CN} + \text{CD}_3\text{CN}$): -13.88 ppm. (Figure S23). IR (ATR, cm^{-1}): 1846(s), 1482 (m), 1462 (m), 1380 (w), 1151 (w), 1089 (m), 1036 (m), 956 (s), 884 (m), 793 (vs), 658 (m), 613 (w), 606 (w), 590 (w), 578 (w), 569 (w), 554 (w). EA, found C,H,N (%): 16.4, 3.1, 1.5; calc C,H,N (%): 16.3, 3.1, 1.6.

Synthesis of $(\text{Bu}_4\text{N})_4[\text{PW}_{11}\text{O}_{39}\{\text{Ru}(\text{CH}_3\text{CN})\}]$ (Ru-CH₃CN**):** 0.1 g (0.028 mmol) of $(\text{Bu}_4\text{N})_4[\text{PW}_{11}\text{O}_{39}\{\text{Ru}(\text{NO})\}]$ was dissolved in 10 mL of CH_3CN . $(\text{Bu}_4\text{N})_4[\text{PW}_{11}\text{O}_{39}\{\text{Ru}(\text{CH}_3\text{CN})\}]$ was generated by photolysis for 90 min. The solid product was obtained by precipitation with diethyl ether. Yield: 0.07 g (64%). ^{31}P NMR ($\text{CH}_3\text{CN} + \text{CD}_3\text{CN}$): -13.57 ppm. (Figure S24). IR (ATR, cm^{-1}): 1482 (m), 1465 (m), 1378 (w), 1152 (w), 1079 (m), 1045 (m), 954 (s), 879 (s), 784 (vs), 626 (m), 613 (m), 598 (w), 587 (m), 578 (w), 563 (w), 556 (w). EA, found C,H,N (%): 20.8, 3.6, 2.0; calc C,H,N (%): 20.9, 3.9, 1.8.

Reaction of Ru-CH₃CN with NaN_3 in acetonitrile: Crude sodium azide (0.017 g, 0.26 mmol) was added to the solution of freshly prepared $(\text{Bu}_4\text{N})_4[\text{PW}_{11}\text{O}_{39}\{\text{Ru}(\text{CH}_3\text{CN})\}]$ (0.100 g, 0.026 mmol) in 10 mL of CH_3CN . The reaction mixture was kept at 70°C upon stirring for 18 h. After cooling to room temperature, white precipitate was filtered off. The resulting product was isolated by vapor diffusion of Et_2O . Yield: 0.70 g.

Reaction of Ru-CH₃CN with NaN_3 in nitromethane: 0.120 g (0.032 mmol) of $(\text{Bu}_4\text{N})_4[\text{PW}_{11}\text{O}_{39}\{\text{Ru}(\text{CH}_3\text{CN})\}]$ was dissolved in 7 mL of CH_3NO_2 . Then, 0.044 g (0.64 mmol) of solid NaN_3 was added to the solution. The resulting mixture was transferred into a Teflon-lined Parr autoclave and kept at 100°C for 18 h. The formed precipitate was filtered off, and the reaction product was isolated by the addition of diethyl ether. Yield: 0.092 g. IR (ATR, cm^{-1}): 1477 (m), 1469 (m), 1376 (w), 1150 (w), 1077 (s), 1047 (m), 970 (s), 955 (s), 888 (sh), 880 (s), 798 (sh), 784 (vs), 773 (vs), 657 (s), 627 (s), 594 (m), 580 (m), 559 (m).

4. Conclusions

This manuscript summarized our studies of Ru-atom reactivity inside the POM backbone toward azide anion. We detected two reaction pathways resulting in (i) azide-acetonitrile click reaction and (ii) azide decomposition. The first one produces coordinated tetrazole and the second generates a complex with coordinated N_2 . Such reactivity is important for organic substrate transformation and N_2 activation. Further studies in these directions are in progress.

Supplementary Materials: The following are available online, Figure S1: Full spectrum of **Ru-NO** (calculated patterns have negative intensities), Figure S2: Zoomed 1637–1661 m/z region of spectrum of **Ru-NO** (calculated isotopic patterns have negative intensities), Figure S3: Zoomed 931–942 m/z and 1011–1023 m/z regions of spectrum of **Ru-NO** (calculated isotopic patterns have negative intensities), Table S1: Peak assignment for ESI-MS spectrum of **Ru-NO**, Figure S4: Full spectrum of **Ru-CH₃CN** (calculated patterns have negative intensities), Table S2: Peak assignment for ESI-MS spectrum of **Ru-CH₃CN**, Figure S5: Zoomed 1643–1670 m/z region of spectrum of **Ru-CH₃CN** (calculated isotopic patterns have negative intensities), Figure S6: Zoomed 1014–1027 m/z region of spectrum of **Ru-CH₃CN** (calculated isotopic patterns have negative intensities), Figure S7: The FT-IR of **Ru-NO** (gray), **Ru-CH₃CN** (red) and **Ru-Tz + Ru-N₃** (blue), Figure S8: Zoomed 1200–550 cm^{-1} region of IR spectra, Figure S9: Spectrum of **Ru-Tz + Ru-N₃** (black) and 1st derivative (red), Figure S10: Full spectrum of **Ru-N₃** and **Ru-CH₃CN** (calculated patterns have negative intensities), Figure S11: Zoomed 949–968 m/z region of spectrum of **Ru-N₃** and **Ru-CH₃CN** (calculated isotopic patterns have negative intensities), Figure S12: Zoomed 1011–1053 m/z region of spectrum of **Ru-N₃** and **Ru-CH₃CN** (calculated isotopic patterns have negative intensities), Figure S13: Zoomed 1108–1123 m/z region of spectrum of **Ru-N₃** and **Ru-CH₃CN** (calculated isotopic patterns have negative intensities), Figure S14: Zoomed 1644–1695 m/z region of spectrum of **Ru-N₃** and **Ru-CH₃CN** (calculated isotopic patterns have negative intensities), Figure S15: Zoomed 1786–1804 m/z region of spectrum of **Ru-N₃** and **Ru-CH₃CN** (calculated isotopic patterns have negative intensities), Table S3: Peak assignment for ESI-MS spectrum of **Ru-N₃** and **Ru-CH₃CN**, Figure S16: Full spectrum of **Ru-N₃** and **Ru-Tz** (calculated patterns have negative intensities), Figure S17: Zoomed 930–961 m/z region of spectrum of **Ru-N₃** and **Ru-Tz** (calculated isotopic patterns have negative intensities), Figure S18: Zoomed 1011–1036 m/z region of spectrum of **Ru-N₃** and **Ru-Tz** (calculated isotopic patterns have negative intensities), Figure S19: Zoomed 1536–1550 m/z region of spectrum of **Ru-N₃** and **Ru-Tz** (calculated isotopic patterns have negative intensities), Figure S20: Zoomed 1636–1691 m/z region of spectrum of **Ru-N₃** and **Ru-Tz** (calculated isotopic patterns have negative

intensities), Figure S21: Zoomed 1759–1776 m/z region of spectrum of **Ru-N₃** and **Ru-Tz** (calculated isotopic patterns have negative intensities), Table S4: Peak assignment for ESI-MS spectrum of **Ru-N₃** and **Ru-Tz**, Figure S22. The Raman spectrum of the solid mixture isolated after the Reaction of **Ru-CH₃CN** with NaN₃, Figure S23: ³¹P NMR spectrum of (Bu₄N)₃H[PW11O₃₉{Ru(NO)}] in the mixture of CH₃CN + CD₃CN (−13.88 ppm), Figure S24: ³¹P NMR spectrum of (Bu₄N)₄[PW11O₃₉{Ru(CH₃CN)}] in the mixture of CH₃CN + CD₃CN (−13.57 ppm).

Author Contributions: Experiment, A.A.M.; CV data, A.L.G.; HR-ESI-MS, V.V.Y.; writing—original draft preparation, P.A.A; supervision, M.N.S. All authors have read and agreed to the published version of the manuscript.

Funding: This research was supported by Russian Science Foundation (grant number 19-73-10027).

Acknowledgments: Authors thank B.A. Kolesov (NIIC SB RAS) for Raman spectra measurements and N.B. Kompankov (NIIC SB RAS) for recording of NMR spectra. V.Y. thanks Ministry of Science and Higher Education of the RF for the access to MS equipment.

Conflicts of Interest: The authors declare no conflict of interest.

References

1. Izarova, N.V.; Pope, M.T.; Kortz, U. Noble metals in polyoxometalates. *Angew. Chem. Int. Ed.* **2012**, *51*, 9492–9510.
2. Putaj, P.; Lefebvre, F. Polyoxometalates containing late transition and noble metal atoms. *Coord. Chem. Rev.* **2011**, *255*, 1642–1685.
3. Bagno, A.; Bonchio, M.; Sartorel, A.; Scorrano, G. Microwave-Assisted Rapid Incorporation of Ruthenium into Lacunary Keggin-Type Polyoxotungstates: One-Step Synthesis, 99Ru, 183W NMR Characterization and Catalytic Activity of [PW11O₃₉RuII(DMSO)]⁵⁻. *Eur. J. Inorg. Chem.* **2000**, *2000*, 17–20.
4. Neumann, R.; Abu-Gnim, C. Alkene oxidation catalyzed by a ruthenium-substituted heteropolyanion, SiRu(L)W11O₃₉: The mechanism of the periodate-mediated oxidative cleavage. *J. Am. Chem. Soc.* **1990**, *112*, 6025–6031.
5. Steckhan, E.; Kandzia, C. Ruthenium-Catalysed, Electrochemical Cleavage of Aryl Olefins for the Synthesis of Benzaldehydes. *Synlett* **1992**, *1992*, 139–140.
6. Murakami, M.; Hong, D.; Suenobu, T.; Yamaguchi, S.; Ogura, T.; Fukuzumi, S. Catalytic Mechanism of Water Oxidation with Single-Site Ruthenium–Heteropolytungstate Complexes. *J. Am. Chem. Soc.* **2011**, *133*, 11605–11613.
7. Ogo, S.; Miyamoto, M.; Ide, Y.; Sano, T.; Sadakane, M. Hydrothermal and solid-state transformation of ruthenium-supported Keggin-type heteropolytungstates [XW11O₃₉{Ru(ii)(benzene)(H₂O)}]ⁿ⁻ (X = P ($n = 5$), Si ($n = 6$), Ge ($n = 6$)) to ruthenium-substituted Keggin-type heteropolytungstates. *Dalton Trans.* **2012**, *41*, 9901–9907.
8. Sadakane, M.; Rinn, N.; Moroi, S.; Kitatomi, H.; Ozeki, T.; Kurasawa, M.; Itakura, M.; Hayakawa, S.; Kato, K.; Miyamoto, M.; et al. Preparation and structural characterization of RuII-DMSO and RuIII-DMSO-substituted α -Keggin-type phosphotungstates, [PW11O₃₉RuIIDMSO]⁵⁻ and [PW11O₃₉RuIIIDMSO]⁴⁻, and catalytic activity for water oxidation. *Z. Anorg. Allg. Chem.* **2011**, *637*, 1467–1474.
9. Sartorel, A.; Miró, P.; Carraro, M.; Berardi, S.; Bortolini, O.; Bagno, A.; Bo, C.; Bonchio, M. Oxygenation by Ruthenium Monosubstituted Polyoxotungstates in Aqueous Solution: Experimental and Computational Dissection of a Ru(III)-Ru(V) Catalytic Cycle. *Chem. Eur. J.* **2014**, *20*, 10932–10943.
10. Rong, C.; Pope, M.T. Lacunary polyoxometalate anions are pi.-acceptor ligands. Characterization of some tungstoruthenate(II,III,IV,V) heteropolyanions and their atom-transfer reactivity. *J. Am. Chem. Soc.* **1992**, *114*, 2932–2938.
11. Yokoyama, A.; Ohkubo, K.; Ishizuka, T.; Kojima, T.; Fukuzumi, S. Remarkable enhancement of catalytic activity of a 2 : 1 complex between a non-planar Mo(v)-porphyrin and a ruthenium-substituted Keggin-type heteropolyoxometalate in catalytic oxidation of benzyl alcohols. *Dalton Trans.* **2012**, *41*, 10006–10013.
12. Bart, J.C.; Anson, F.C. Coordination, electron transfer and catalytic chemistry of a ruthenium-substituted heteropolytungstate anion as revealed in its electrochemical behavior. *J. Electroanal. Chem.* **1995**, *390*, 11–19.
13. Khenkin, A.M.; Efremenko, I.; Weiner, L.; Martin, J.M.L.; Neumann, R. Photochemical Reduction of Carbon Dioxide Catalyzed by a Ruthenium-Substituted Polyoxometalate. *Chem. Eur. J.* **2010**, *16*, 1356–1364.
14. Shi, D.; He, C.; Qi, B.; Chen, C.; Niu, J.; Duan, C. Merging of the photocatalysis and copper catalysis in metal–organic frameworks for oxidative C–C bond formation. *Chem. Sci.* **2015**, *6*, 1035–1042.

15. Sadakane, M.; Moroi, S.; Iimuro, Y.; Izarova, N.; Kortz, U.; Hayakawa, S.; Kato, K.; Ogo, S.; Ide, Y.; Ueda, W.; et al. Stabilization of high-valence ruthenium with silicotungstate ligands: Preparation, structural characterization, and redox studies of ruthenium(III)-substituted α -keggin-type silicotungstates with pyridine ligands, $[\text{SiW}_{11}\text{O}_{39}\text{Ru}^{\text{III}}(\text{Py})]^{5-}$. *Chem. Asian J.* **2012**, *7*, 1331–1339.
16. Ogo, S.; Moroi, S.; Ueda, T.; Komaguchi, K.; Hayakawa, S.; Ide, Y.; Sano, T.; Sadakane, M. Preparation of tetrabutylammonium salt of a mono-Ru(III)-substituted α -Keggin-type silicotungstate with a 4,4'-bipyridine ligand and its electrochemical behaviour in organic solvents. *Dalton Trans.* **2013**, *42*, 7190.
17. Sadakane, M.; Tsukuma, D.; Dickman, M.H.; Bassil, B.; Kortz, U.; Higashijima, M.; Ueda, W. Structural characterization of mono-ruthenium substituted Keggin-type silicotungstates. *Dalton Trans.* **2006**, 4271–4276, doi.org/10.1039/B606266K
18. Ogo, S.; Shimizu, N.; Ozeki, T.; Kobayashi, Y.; Ide, Y.; Sano, T.; Sadakane, M. Determination of α -Keggin structure of $[\text{GeW}_{11}\text{O}_{39}\text{Ru}^{\text{III}}(\text{H}_2\text{O})]^{5-}$. Reaction of $[\text{GeW}_{11}\text{O}_{39}\text{Ru}^{\text{III}}(\text{H}_2\text{O})]^{5-}$ with dimethyl sulfoxide to form $[\text{GeW}_{11}\text{O}_{39}\text{Ru}^{\text{III}}(\text{dmsO})]^{5-}$ and their structural characterization. *Dalton Trans.* **2013**, *42*, 2540–2545.
19. Filipek, K. Synthesis, characterization and reactivity of ruthenium complexes of the lacunary Keggin polyoxoanion: $[\text{SiW}_{11}\text{O}_{39}\text{RuL}]^{n-}$, L = H₂O, NO, N₂. *Inorg. Chim. Acta* **1995**, *231*, 237–239.
20. Sokolov, M.N.; Adonin, S.A.; Mainichev, D.A.; Sinkevich, P.L.; Vicent, C.; Kompankov, N.B.; Gushchin, A.L.; Nadolnny, V.A.; Fedin, V.P. New $[\text{RuNO}]$ Polyoxometalate $[\text{PW}_{11}\text{O}_{39}\text{Ru}^{\text{II}}(\text{NO})]^{4-}$: Synthesis and Reactivity. *Inorg. Chem.* **2013**, *52*, 9675–9682.
21. Shmakova, A.A.; Volchek, V.V.; Abramov, P.A.; Sokolov, M.N. Reaction of $\text{K}_2[\text{Ru}(\text{NO})\text{Cl}_5]$ with $\text{K}_8[\gamma\text{-SiW}_{10}\text{O}_{36}]$ Under Hydrothermal Conditions: Synthesis of $[\text{SiW}_{11}\text{O}_{39}\{\text{Ru}(\text{NO})\}]^{5-}$. *J. Struct. Chem.* **2018**, *59*, 1427–1432.
22. Liu, B.; Yan, J.; Wang, Y.-F.; Yi, X.-Y. Redox chemistry of ruthenium ions in mono-substituted Keggin tungstophosphate: A new synthetic extension for ruthenium derivatives based on $[\text{PW}_{11}\text{O}_{39}\text{Ru}^{\text{VI}}\text{N}]^{4-}$. *Dalton Trans.* **2015**, *44*, 16882–16887.
23. Sadakane, M.; Iimuro, Y.; Tsukuma, D.; Bassil, B.S.; Dickman, M.H.; Kortz, U.; Zhang, Y.; Ye, S.; Ueda, W. Carbonyl-ruthenium substituted α -Keggin-tungstosilicate, $[\alpha\text{-SiW}_{11}\text{O}_{39}\text{Ru}^{\text{II}}(\text{CO})]^{6-}$: Synthesis, structure, redox studies and reactivity. *Dalton Trans.* **2008**, 6692–6698, doi.org/10.1039/B810987G.
24. Nishiki, K.; Ota, H.; Ogo, S.; Sano, T.; Sadakane, M. Preparation and Structural Characterization of Mono-Ru-Substituted α -Dawson-Type Phosphotungstate with a Carbonyl Ligand and Other Ru(CO)-Substituted Heteropolytungstates. *Eur. J. Inorg. Chem.* **2015**, *2015*, 2714–2723.
25. Vicent, C.; Adonin, S.A.; Anyushin, A.V.; Mainichev, D.A.; Sokolov, M.N. Gas-Phase Fragmentation Reactions of Keggin-Type $\{\text{PW}_{11}\text{O}_{39}\text{M}\}$ (M = Rh, Ir, and Ru) Polyoxometalates as Fingerprints of the Ligands Attached at the Noble Metal Site. *Eur. J. Inorg. Chem.* **2014**, *2014*, 5618–5624.
26. Sadakane, M.; Tsukuma, D.; Dickman, M.H.; Bassil, B.S.; Kortz, U.; Capron, M.; Ueda, W. Dimerization of mono-ruthenium substituted α -Keggin-type tungstosilicate $[\alpha\text{-SiW}_{11}\text{O}_{39}\text{Ru}^{\text{III}}(\text{H}_2\text{O})]^{5-}$ to μ -oxo-bridged dimer in aqueous solution: Synthesis, structure, and redox studies. *Dalton Trans.* **2007**, 2833–2838, doi.org/10.1039/B702813J
27. Sadakane, M.; Higashijima, M. Synthesis and electrochemical behavior of $[\text{SiW}_{11}\text{O}_{39}\text{Ru}^{\text{III}}(\text{H}_2\text{O})]^{5-}$ and its oxo-bridged dimeric complex $[\text{SiW}_{11}\text{O}_{39}\text{Ru}^{\text{IV}}\text{Ru}^{\text{III}}\text{SiW}_{11}\text{O}_{39}]^{11-}$. *Dalton Trans.* **2003**, 659–664, doi.org/10.1039/B209562A
28. Sokolov, M.N.; Adonin, S.A.; Sinkevich, P.L.; Vicent, C.; Mainichev, D.A.; Fedin, V.P. Organometallic derivatives of Rh- and Ir-substituted polyoxotungstates with Keggin structure: Reactivity screening by electrospray ionization mass-spectrometry. *Dalton Trans.* **2012**, *41*, 9889–9892.
29. Sokolov, M.N.; Adonin, S.A.; Mainichev, D.A.; Vicent, C.; Zakharchuk, N.F.; Danilenko, A.M.; Fedin, V.P. Synthesis and characterization of $[\text{PW}_{11}\text{O}_{39}\text{Ir}(\text{H}_2\text{O})]^{4-}$: Successful incorporation of Ir into polyoxometalate framework and study of the substitutional lability at the Ir(III) site. *Chem. Commun.* **2011**, *47*, 7833–7835.
30. Sokolov, M.N.; Adonin, S.A.; Sinkevich, P.L.; Vicent, C.; Mainichev, D.A.; Fedin, V.P. Keggin-type Polyoxometalates $[\text{PW}_{11}\text{O}_{39}\text{MCl}]^{5-}$ with Noble Metals (M = Rh and Ir): Novel Synthetic Entries and ESI-MS Directed Reactivity Screening. *Z. Anorg. Allg. Chem.* **2014**, *640*, 122–127.
31. Mukhacheva, A.A.; Shmakova, A.A.; Volchek, V.V.; Romanova, T.E.; Benassi, E.; Gushchin, A.L.; Yanshole, V.; Sheven, D.G.; Kompankov, N.B.; Abramov, P.A.; et al. Reactions of $[\text{Ru}(\text{NO})\text{Cl}_5]^{2-}$ with pseudotrilocunary $\{\text{XW}_9\text{O}_{33}\}^{9-}$ (X = As III, Sb III) anions. *Dalton Trans.* **2019**, *48*, 15989–15999.

32. Blackman, A. Reactions of Coordinated Ligands. In *Advances in Heterocyclic Chemistry*, V. 58; Academic Press: San Diego, CA, USA, 1993; pp. 123–170.
33. Kukushkin, V.Y.; Tudela, D.; Pombeiro, A.J.L. Metal-ion assisted reactions of oximes and reactivity of oxime-containing metal complexes. *Coord. Chem. Rev.* **1996**, *156*, 333–362.
34. Bolotin, D.S.; Bokach, N.A.; Kukushkin, V.Y. Coordination chemistry and metal-involving reactions of amidoximes: Relevance to the chemistry of oximes and oxime ligands. *Coord. Chem. Rev.* **2016**, *313*, 62–93.
35. Bolotin, D.S. Reactions of Amidoximes with Metal-Activated Nitriles. *Russ. J. Coord. Chem.* **2018**, *44*, 243–251.
36. Bokach, N.A.; Kukushkin, V.Y. Addition of HO-nucleophiles to free and coordinated nitriles. *Russ. Chem. Rev.* **2005**, *74*, 153–170.
37. Kukushkin, V.Y.; Pombeiro, A.J.L. Additions to Metal-Activated Organonitriles[†]. *Chem. Rev.* **2002**, *102*, 1771–1802.
38. Adams, R.D.; Dawoodi, Z.; Foust, D.F.; Segmueller, B.E. Polynuclear coordination and ligand activation. The structure, bonding, and desulfurization of thioformamido ligands about a trinuclear site. *Organometallics* **1983**, *2*, 315–323.
39. Adams, R.D.; Kiprotich, E.J.; Smith, M.D. Multiple cluster CH activations and transformations of furan by triosmium carbonyl complexes. *Chem. Commun.* **2018**, *54*, 3464–3467.
40. Afonin, M.Y.; Savkov, B.Y.; Virovets, A.V.; Korenev, V.S.; Golovin, A.V.; Maksakov, V.A. Transformation of Chlorohydrocarbons and Amines in the Coordination Sphere of $[(\mu\text{-H})_2\text{Os}_3(\text{CO})_{10}]$. *Eur. J. Inorg. Chem.* **2017**, *2017*, 3105–3114.
41. Afonin, M.J.; Maksakov, V.A.; Kirin, V.P.; Scheludyakova, L.A.; Golovin, A.V.; Vasil'ev, V.G. Transformations of allylamine and N-allylacetamide on triosmium cluster complexes with hemilabile ligands. *Polyhedron* **2009**, *28*, 2754–2758.
42. Whitmire, K.H. Iron Compounds without Hydrocarbon Ligands. In *Comprehensive Organometallic Chemistry II*; Pergamon Press: London, UK, 1995; pp. 1–99.
43. Adams, R.D.; Selegue, J.P. Osmium. In *Comprehensive Organometallic Chemistry*; Pergamon Press: London, UK, 1982; pp. 967–1064.
44. Yersin, H.; Vogler, A. *Photochemistry and Photophysics of Coordination Compounds*; Springer Berlin Heidelberg: Berlin, Heidelberg, Germany, 1987; ISBN 978-3-540-17808-8.
45. Havrylyuk, D.; Deshpande, M.; Parkin, S.; Glazer, E.C. Ru (ii) complexes with diazine ligands: Electronic modulation of the coordinating group is key to the design of “dual action” photoactivated agents. *Chem. Commun.* **2018**, *54*, 12487–12490.
46. Chin, C.P.; Ren, Y.; Berry, J.; Knott, S.A.; McLauchlan, C.C.; Szczepura, L.F. Small molecule activation of nitriles coordinated to the $[\text{Re}_6\text{Se}_8]^{2+}$ core: Formation of oxazine, oxazoline and carboxamide complexes. *Dalton Trans.* **2018**, *47*, 4653–4660.
47. Walther, D.; Ruben, M.; Rau, S. Carbon dioxide and metal centres: From reactions inspired by nature to reactions in compressed carbon dioxide as solvent. *Coord. Chem. Rev.* **1999**, *182*, 67–100.
48. Knowles, C.; Knowles, A. *Standards in Absorption Spectrometry*; Springer: Amsterdam, Netherlands, 1981; ISBN 978-0-412-22470-6.
49. Huisgen, R. Proceedings of the Chemical Society. October 1961. *Proc. Chem. Soc.* **1961**, 357–396. doi.org/10.1039/PS9610000357
50. Meldal, M.; Tornøe, C.W. Cu-Catalyzed Azide–Alkyne Cycloaddition. *Chem. Rev.* **2008**, *108*, 2952–3015.
51. Zhang, L.; Chen, X.; Xue, P.; Sun, H.H.Y.; Williams, I.D.; Sharpless, K.B.; Fokin, V.V.; Jia, G. Ruthenium-Catalyzed Cycloaddition of Alkynes and Organic Azides. *J. Am. Chem. Soc.* **2005**, *127*, 15998–15999.
52. Boren, B.C.; Narayan, S.; Rasmussen, L.K.; Zhang, L.; Zhao, H.; Lin, Z.; Jia, G.; Fokin, V.V. Ruthenium-Catalyzed Azide–Alkyne Cycloaddition: Scope and Mechanism. *J. Am. Chem. Soc.* **2008**, *130*, 8923–8930.
53. McNulty, J.; Keskar, K.; Vemula, R. The First Well-Defined Silver(I)-Complex-Catalyzed Cycloaddition of Azides onto Terminal Alkynes at Room Temperature. *Chem. Eur. J.* **2011**, *17*, 14727–14730.
54. McNulty, J.; Keskar, K. Discovery of a Robust and Efficient Homogeneous Silver(I) Catalyst for the Cycloaddition of Azides onto Terminal Alkynes. *Eur. J. Org. Chem.* **2012**, *2012*, 5462–5470.
55. Allen, A.D.; Senoff, C.V. Nitrogenopentammineruthenium(II) complexes. *Chem. Commun.* **1965**, 621, doi.org/10.1039/C19650000621
56. Ibers, J.A.; Davids, B.R. Bonding of molecular nitrogen. II. Crystal and molecular structure of azidodinitrogenbis(ethylenediamine)ruthenium(II) hexafluorophosphate. *Inorg. Chem.* **1970**, *9*, 2768–2774.

57. Chaudret, B.; Devillers, J.; Poilblanc, R. Preparation, characterization and X-ray crystal structure of Ru₂H₆N₂(PPH₃)₄, a compound containing four bridging hydrides and a ruthenium–ruthenium double bond. *J. Chem. Soc., Chem. Commun.* **1983**, 641–643, doi.org/10.1039/C39830000641
58. Emelyanov, V.A.; Khramenko, S.P.; Belyaev, A.V. Nitrosation of ruthenium chloro complexes. *Russ. J. Inorg. Chem.* **2001**, *46*, 346–351.

Sample Availability: Samples of the compounds are not available from the authors.



© 2020 by the authors. Licensee MDPI, Basel, Switzerland. This article is an open access article distributed under the terms and conditions of the Creative Commons Attribution (CC BY) license (<http://creativecommons.org/licenses/by/4.0/>).